

Research article

Microstructure and electrical properties of Li⁺ ion conducting polymer blend electrolyte films

Rohan Nandeesh Sagar^{1,2}, Ravindrachary Vasachar^{1*}, Shreedatta Hegde¹

¹Department of Physics, Mangalore University, 574199 Mangalagangothri, India

²Adichunchanagiri School of Natural Sciences, Adichunchanagiri University, 571418, India

Received 10 January 2023; accepted in revised form 9 May 2023

Abstract. Solid polymer electrolytes based on polyvinyl alcohol (PVA)–chitosan (CS) polymer blend and Li–salt doped blend electrolyte films are prepared using the solution cast technique. The Fourier transform infrared spectra showed that the absorption peaks shifted in Li–salt doped polymer blend composites compared to pure blend films: indicating the chemical modifications upon doping. From the UV–visible spectra, the spectral absorption response of Li⁺ salt–doped polymer blend composites showed a red shift in the absorption band. The optical band gap of the pure polymer blend decreased upon doping. X–ray diffraction studies showed the dopant-dependent structural modification of pure polymer blend upon doping. SEM images also showed the change in the surface morphology of the pure polymer blend upon doping. The thermogravimetric analysis study revealed that the thermal stability of the pure polymer blend increases with Li₂CO₃ concentration. The ionic conductivity of PVA–CS increases with Li–salt concentration, and the maximum conductivity of $7.70 \cdot 10^{-5} \text{ S} \cdot \text{cm}^{-1}$ is observed for 15 wt% of Li₂CO₃ salt concentration. The transport property study revealed that the ions are the majority conducting charge carriers in polymer blend composite.

Keywords: polymer blends and alloys, structural properties, electrical and transport properties

1. Introduction

Lithium–ion batteries have become a key source of choice not only in the application of portable electronic devices (mobile phones, power banks, and laptops) but also in hybrid electric vehicle applications. In the earlier days, liquid electrolytes were extensively used for battery applications, but these electrolytes are associated with some disadvantages or concerns like leakage and flammability leading to safety hazards. However, this obstacle can be evaded by replacing liquid electrolytes with solid polymer electrolytes (SPEs).

In addition, these SPE materials also provide beneficial properties such as high energy density, flexibility and tunability of the properties of the host as well as improved safety characteristics. Here it is observed that desired chemical and physical properties

of these SPEs can be obtained by doping/blending a polymer with a suitable dopant/polymer. It is known that the change in the property of a polymer composite for SPE depends on the chemical nature of the dopant/blend polymer, the type of polymer and the way in which the dopant interacts with the host polymer. As a result of these tunable properties, the polymer and its composite–based solid polymer electrolytes have become the most efficient and suitable materials for the fabrication of solid–state batteries. Owing to this, many researchers are focusing on polymeric blends and their composites for the fabrication of batteries due to their ease of fabrication and high performance, even at ambient temperatures. In particular, the polymers which are naturally occurring, biocompatible and possessing optimal properties, viz., mechanical, thermal, and high ionic conductivity

*Corresponding author, e-mail: rvavi2000@yahoo.com

© BME-PT

properties (such as chitosan (CS) and methylcellulose, *etc.*) are considered to be interesting materials for blending [1, 2] and organic/inorganic fillers, plasticization, copolymerization are enforced to modulate the ionic conductivity in these polymers. The researchers also noticed that the polymer blending and its composites–based solid polymer blend electrolyte (SPBE) system possess great optical, mechanical, thermal, and high ionic conductivity properties compared to single polymer–based SPE system. To reach this objective, many researchers proposed various synthetic polymeric matrices, such as poly(acrylates), polyvinyl alcohol, elastomers, polythiophenes, and epoxy polymers, *etc.*, as host materials and naturally occurring polymers like chitosan, cellulose, and starch, *etc.* are suggested polymers for the preparing of solid polymer blend electrolyte films (SPBE) [3]. Among all the polymers, polyvinyl alcohol (PVA) and chitosan (CS) based polymer blends and their composites are proposed as the appreciable composite material for the preparation of blend electrolyte systems [4]. The polymer blends and their composites exhibit higher charge storage capacity and possess dopant dependant structural, thermal, and electrical properties. In general, the ionic conductivity within a polymer electrolyte system is strongly influenced by the dopant (LiCl, LiClO₄, and Li₂CO₃, *etc.*) concentration and preparation methods. For example, Salman *et al.* [2] reported the highest electrical conductivity of $3.74 \cdot 10^{-6} \text{ S} \cdot \text{cm}^{-1}$ in 40 wt% LiBF₄ doped chitosan–methylcellulose blend biopolymer electrolyte and Shukur *et al.* [3] observed the highest electrical conductivity of $2.06 \pm 0.39 \cdot 10^{-3} \text{ S} \cdot \text{cm}^{-1}$ at room temperature for 11 wt% chitosan + 7 wt% PEO + 12 wt% NH₄NO₃ sample with 70% ethylene carbonate (EC). Hence, the understanding effect of doping on polymer blend microstructure and modified physic–chemical changes is the topic of current research.

It is also known that the ionic conductivity in polymer/blend composites mainly depends on the presence of charge transfer (CT) complexes occurred due to inter/intra–molecular interaction between the dopant and the polymer. These charge complexes bridge the gap between the neighbouring sites for efficient charge transfer through the polymer backbone. Hence, the ionic conductivity in polymers depends on the chemical nature of the repeating units in the polymer chain, the electronic structure, and the segmental motion of the polymer backbone. Here the dopant

makes the polymer backbone more flexible, which helps to transfer mobile charge carriers from one conducting site to another. In other words, the dopant starts bridging between two localized sites of the polymer in the form of a CT complex, which leads to lowering the potential barrier between the two sites and facilitates more and more mobile charge carriers to transfer within the electrolyte systems. A polymer blend is a homogeneous mixture of two or more polymers, which can modulate the microstructure of the host material. The change in microstructural properties of polymer blends is depending on the characteristic features of each polymer and the blending concentrations. The main aim of polymer blending is to prepare the blend materials which conquer unique structural, good thermal and high electrical properties. When two or more suitable polymers are mixed with a suitable volume of solvent, inter/intramolecular interaction will take place, and these chemical interactions will affect the physical properties of the host or guest polymer. As a result, one can expect the enhancement of other properties in addition to electrical conductivity in the prepared polymer blend and its composites [4–6].

Polyvinyl alcohol (PVA) is a vinyl polymer possessing semicrystalline nature and also high T_g due to the existence of a solid pyrrolidone group which is familiar with forming distinctive complexes with various polymers and dopants. It has an excellent capacity of charge storage, and it exhibits dopant–dependent structural and electrical properties. The conductivity of PVA enhances due to the high rate of physical and chemical interactions through inter/ intramolecular interaction between functional groups of PVA and the dopant. These interactions form charge complexes and facilitate more and more ions transfer from one conductive site to another; hence conductivity enhances in the polymer composites [7, 8].

Unlike PVA polymer, chitosan is a naturally occurring polymer, and it comprises β –(1→4)–2–amino–2–deoxy–D–glucosamine, which is a derivative of chitin with a high degree of *N*–acetylation. Especially it is a copolymer of D–glucosamine and *N*–acetyl–D–glucosamine, and it is a naturally occurring mucopolysaccharide. Chitosan polymer exhibits a few eco–friendly properties such as nontoxicity, biodegradability, and excellent biocompatibility, and it also has adhesiveness properties, *etc.* which came from alkaline deacetylation of chitin [9–11]. Chitosan is a semicrystalline polymer, and its degree of

crystallinity is the function of the degree of deacetylation, and it can be degraded through enzymatic hydrolysis. Since chitosan is a biodegradable polymer, it drives it into technological applications such as tissue engineering, drug delivery, electrochromic devices, and membrane systems as a biomaterial, and its antigenicity behaviour avail it as a biomaterial in biomedical applications [10, 12–14]. Khair *et al.* [11] achieved the highest ionic conductivity of about $8.91 \cdot 10^{-7} \text{ S} \cdot \text{cm}^{-1}$ was achieved in 50 wt% ammonium triflate ($\text{NH}_4\text{CF}_3\text{SO}_3$) doped with chitosan-based polymer electrolyte system at room temperature. Hence PVA and chitosan are considered congenial polymers for the blending process. Since both the polymers are miscible to each other, the ionic complexation takes place between chitosan and PVA polymers through the hydroxyl groups of PVA and amine groups of chitosan polymer [4–6]. In this context, many researchers have paid great attention to chitosan polymer/polymer blend composite as a biological and technological active source [11, 15]. Hence in the present work, PVA and chitosan polymer blend are used as a host, and Li_2CO_3 as a dopant for the preparation of blend composite and the modified optical, structural, morphological, thermal, electrical, and transport properties of solid polymer blend electrolyte (SPBE) system was intensively studied using various techniques.

2. Experimental methods

2.1. Materials

The polymers polyvinyl alcohol (PVA), chitosan (CS) and the dopant lithium carbonate (Li_2CO_3) salt used in the present work are procured from M/s Sigma Aldrich, Bangalore, India. Pure PVA–CS polymer blend and Li_2CO_3 doped blend polymer composite films are prepared using a standard solution casting method. Here 0.8 gm of chitosan was gently added to 40 ml of double distilled water containing 1% of acetic acid under stirring (16 hours) to make 2% (w/v) chitosan solution. 2 mg of PVA was dissolved separately in 40 ml of double distilled water and stirred for 1 hr at 40°C , after getting homogeneous solution the temperature is turned off again stirred for 16 hours to make 5% (w/v) PVA solution.

The prepared 5% PVA solution and 2% chitosan solution were mixed with a 50/50 ratio and again stirred for 12 hours to get a homogeneous solution. This homogeneous solution was poured into pure

Petri plates and left to dry at room temperature to get PVA–CS polymer blend film. Similarly, Li_2CO_3 salt-doped PVA–CS polymer blend electrolyte films are prepared by dissolving different concentrations of Li_2CO_3 (5, 10, and 15 wt%) separately in 10 ml double distilled water and stirred for 30 min. Finally, different concentration of the salt-dissolved solution is added to the 50/50 ratio of PVA–CS solution in separate beakers. The solution was again stirred for 6 h and gently poured into a dry petri dish. The samples are dried in a hot air oven for 24 h to get the free-standing films.

2.2. Characterization techniques

Fourier transform infrared (FTIR) spectra were recorded using an IR–Prestige 21FTIR spectrophotometer (Shimadzu, Kyoto, Japan) to identify the possible chemical modifications within the polymer composite in the range $400\text{--}4000 \text{ cm}^{-1}$ with a resolution of 4 cm^{-1} to analyze for pure and Li-salt doped polymer composites (six samples). The optical absorption spectra of PVA-CS and Li-salt doped PVA-CS polymer composites were obtained using an Ultraviolet (UV)–visible 1800 spectrophotometer (Shimadzu, Kyoto, Japan) in the wavelength range 190–900 nm. X-ray diffraction (XRD) spectra were performed by using the Rigaku Miniflex–600 (Tokyo, Japan) benchtop X-ray diffractometer, where Cu-K_α generates the X-rays with $\lambda = 1.5406 \text{ \AA}$ with the glancing angle 2θ range from $5\text{--}70^\circ$ with the step size of 0.02° and scanning rate 10 per min. The surface morphology of prepared electrolyte films is observed by Carl Zeiss scanning electron microscope (SEM) (Carl Zeiss AG, Jena, Germany). Thermal properties of the polymer blend electrolyte films are studied using a universal TA–SDT Q600 instrument (Bangalore, India) in the temperature range of $25\text{--}600^\circ\text{C}$ with a scanning speed rate of $10^\circ\text{C}/\text{min}$. The electrical properties of the samples are measured using an Agilent 4294A precision impedance analyzer (Santa Clara, California) with a frequency range of 40 Hz–5 MHz using the two-probe method. Here the prepared electrolyte films were sandwiched between two silver (Ag) blocking electrodes (2.5 mm diameter) with constant pressure to maintain better interfacial contact between the electrode and electrolyte, and the conductivity of pure and Li–salt doped polymer blend electrolyte films were carried out at an ambient temperature. Also, the temperature-dependent conductivity

of the high-conducting solid polymer blend electrolyte film is studied for different temperatures using an Agilent 4294A precision impedance analyzer (Santa Clara, California).

3. Results and discussions

3.1. FTIR

FTIR study is a powerful tool used to inspect the chemical complexation between polymers and the dopant. FTIR spectra of pure and salt-doped polymer blends are shown in Figure 1, and the corresponding band assignment is presented in Table 1. Pure PVA–CS polymer blend exhibiting a broad band at 3290 cm^{-1} is assigned to (–OH) stretching vibrations related to PVA polymer. Another absorption band is observed at 2923 cm^{-1} which is concerned with $-\text{CH}_2$ asymmetric stretching of PVA polymer. Peak observed at 1647 cm^{-1} related to amide I and III groups of C=O stretching vibrations of chitosan. The peak corresponding to the N–H (deformation) bending of the $-\text{NH}_2$ group is located at 1557 cm^{-1} . Nevertheless, two more peaks are observed at 1417 and 1357 cm^{-1} , which is assigned to the existence of

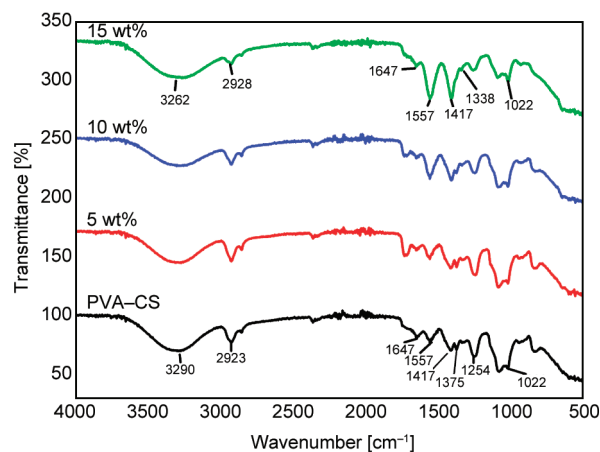


Figure 1. FTIR spectra of pure and Li_2CO_3 (5, 10, and 15 wt%) doped PVA–CS polymer blend electrolyte films.

carboxylic acid and CH_2 wagging. The peak located at 1254 cm^{-1} is related to C–H vibrations within the polymer blend, and a weak absorption band is observed at 1022 cm^{-1} , which is attributed to the (C–N) stretching peak of the PVA–CS polymer blend.

In a salt-doped polymer blend composite, the band corresponding to a hydroxyl group (–OH) located at 3290 cm^{-1} is shifted to a lower wave number and becomes shallow upon doping. The second peak observed at 2923 cm^{-1} is shifted to 2928 cm^{-1} as well as a decrease in its intensity with an increase in salt concentration. In blend composite films, the peaks observed at 1557 , 1417 , 1254 , and 1022 cm^{-1} exhibit the change in their intensities upon doping. The modification in the observed band is mainly due to inter/intra-molecular interaction between the dopant and the functional groups of the polymer blend [2]. The peak observed at 1375 cm^{-1} for the pure polymer blend is shifted to 1338 cm^{-1} in the composite. The changes in peak position and peak intensities in salt-doped blend composites are mainly due to the complexation of Li^+ ions and the oxygen or nitrogen atoms of the hydroxyl or amine group of the polymer blend. Here, the chemical interaction takes place between the hydroxyl group of PVA polymer with Li^+ ion of Li_2CO_3 salt and also between amine groups of chitosan with CO_3^- of Li_2CO_3 salt [15, 16].

3.2. UV–visible studies

The UV–visible absorption spectrum is one of the simple and effective methods used to study the band structure and optical energy band gap (E_g) in solid materials. The UV–visible absorption spectra of pure and Li–salt doped polymer blend electrolyte films are displayed in Figure 2. In the above plot, the pure polymer blend exhibits two absorption bands at 206 and 303 nm. The first peak observed at 206 nm is assigned to the $n \rightarrow \pi^*$ transition formed due to the

Table 1. Peak positions and peak assignments of pure and Li–salt doped polymer blend composites.

Wavenumbers [cm ⁻¹]		Peak assignments
PVA–CS	Li_2CO_3 (15 wt%)	
3290	3262	O–H stretching vibration
2923	2928	$-\text{CH}_2$ asymmetric stretching vibration
1647	–	Amide I and III groups of C=O stretching vibrations
1557	Increase in intensity	N–H bending of $-\text{NH}_2$ group
1417	Increase in intensity	Carboxylic group
1375	1338	Wagging of CH_2 vibration
1254	Decrease in intensity	C–H vibrations
1022	Decrease in intensity	C–N stretching peak

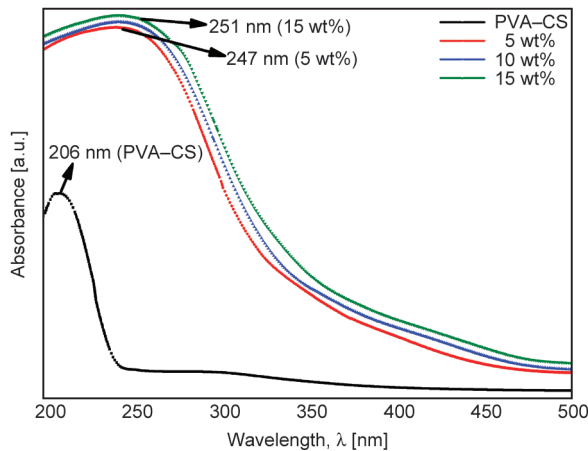


Figure 2. UV-Visible absorption spectra of pure and Li-salt doped blend composites.

unsaturated molecules within the polymer blend matrix. The second peak observed at 303 nm is assigned to $\pi \rightarrow \pi^*$ transitions [5].

In blend composite films, the absorption bands and the band edges are shifted towards higher wavelengths with variant absorption intensities. Here the absorption band of the pure polymer blend observed at 206 nm suffered a slight shift towards a higher wavelength (red shift) that provides delocalization of charge carriers through polymer blend composite chains. The absorption band observed at 303 nm disappeared in the salt-doped blend composites. The shift and disappearance of the absorption band and enhancement in their intensities are attributed to the formation of localized occupied states in the band gap. These changes in peak position and intensities are due to inter/intra-molecular hydrogen bonding interactions between the functional groups of Li-salt and PVA-CS polymer blend and suggest the formation of charge transfer complexes (FTIR results). The observed modification in the absorption band and band edge also reflects the absorption of radiation is directly related to the number of absorbing molecules within the samples [17, 18]. These changes also affect the crystal structure of the blend, which will ultimately affect the band structure and optical energy band gap (E_g).

The absorption of light by the optical medium is determined by its absorption coefficient (α), and is calculated using Equation (1):

$$\alpha = \frac{2.303A}{d} \quad (1)$$

where A is the absorbance and d is the thickness of pure and blend composite samples. It is well known

that the classical Tauc's assertion, which relates the absorption coefficient (α) and optical energy band gap (E_g). Accordingly, the optical energy band gap (E_g) is determined by converting the obtained UV-visible absorbance spectra into Tauc's plot by using a frequency-dependent absorption coefficient as represented by Mott and Devis equation [12] (Equation (2)):

$$\alpha(\nu) = \frac{\beta(h\nu - E_g)^r}{h\nu} \quad (2)$$

where β is a constant (band tail parameter) and exponent r is an empirical index that is equal to 2 for indirectly allowed transitions, and in a quantum mechanical sense, this is responsible for the optical absorption. Linear behaviour of the plotted graph of $(\alpha h\nu)^{1/2}$ versus the photon energy ($h\nu$) at room temperature signifies the indirectly allowed transitions. Further extrapolating the linear portion of the curve on photon energy ($h\nu$) gives the optical energy band gap (E_g) values (Figure 3a). Using this method E_g values for pure and doped blend composites are estimated, and the variation of E_g with dopant concentration is given in Figure 3b.

From the Figure 3b, it is observed that in blend composites, as the doping level increases, the E_g value decreases (*i.e.* from 4.82 to 2.85 eV). This decrease in E_g values is mainly due to the presence of complexes within the composite films, which arises due to the interaction of dopant with polymer and also due to the salt dissociation within the polymer blend.

Since the number of complexes within the blend composite increases with dopant concentration, it leads to a change in the microstructure of the PVA-CS polymer blend; as a result, a decrease in optical energy band gap (E_g) is expected in blend composites. To understand the structural nature further, the optical activation energy of polymer blend composites is determined by using Urbach's energy (E_u) Equation (3):

$$\alpha = \alpha_0 \exp\left(\frac{h\nu}{E_a}\right) \quad (3)$$

where α_0 is a constant and E_a is the activation energy (energy that causes a conduction mechanism within the system). The Urbach's rule conveys the exponential dependency of $\alpha(\nu)$ on photon energy ($h\nu$), also the Urbach's energy illustrates the disorder that occurred within the electrolyte system and is generally understood by the width of band tail of localized states in the forbidden gaps [18].

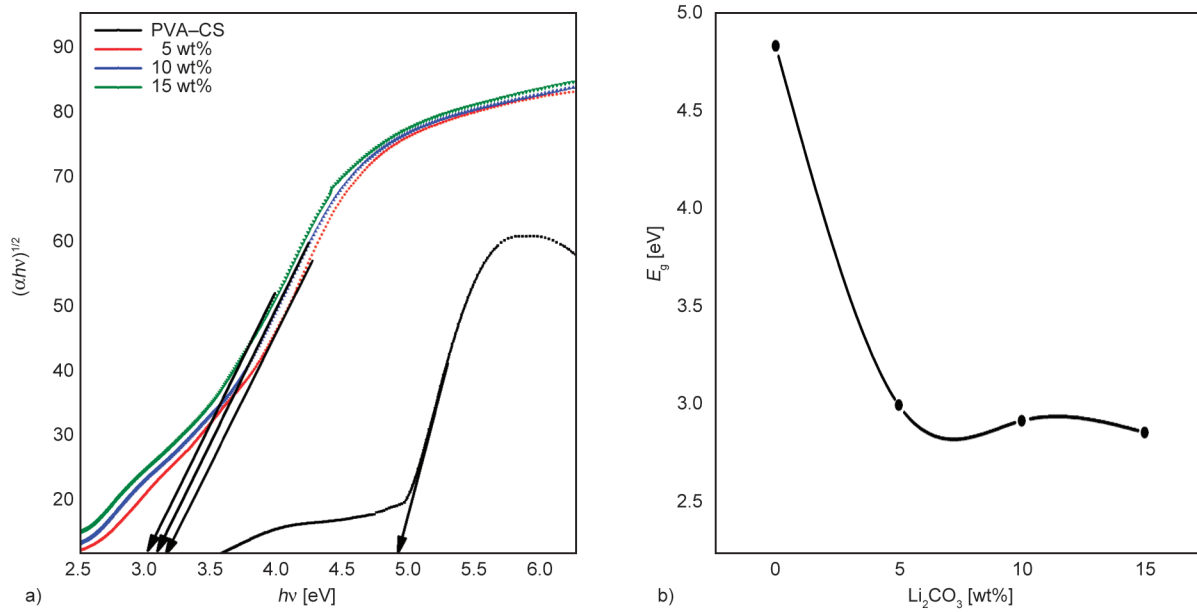


Figure 3. a) Variation of $(\alpha h\nu)^{1/2}$ with $h\nu$ (photon energy) for pure and doped PVA–CS blend composite films, b) optical energy band gap (E_g) vs. Li_2CO_3 doping concentrations.

The Urbach’s energy for pure blend composite is obtained by plotting the graph of the exponential of

$\alpha(\nu)$ versus photon energy (Figure 4a) and by a fitted curve of the linear region (Figure 4b). The estimated

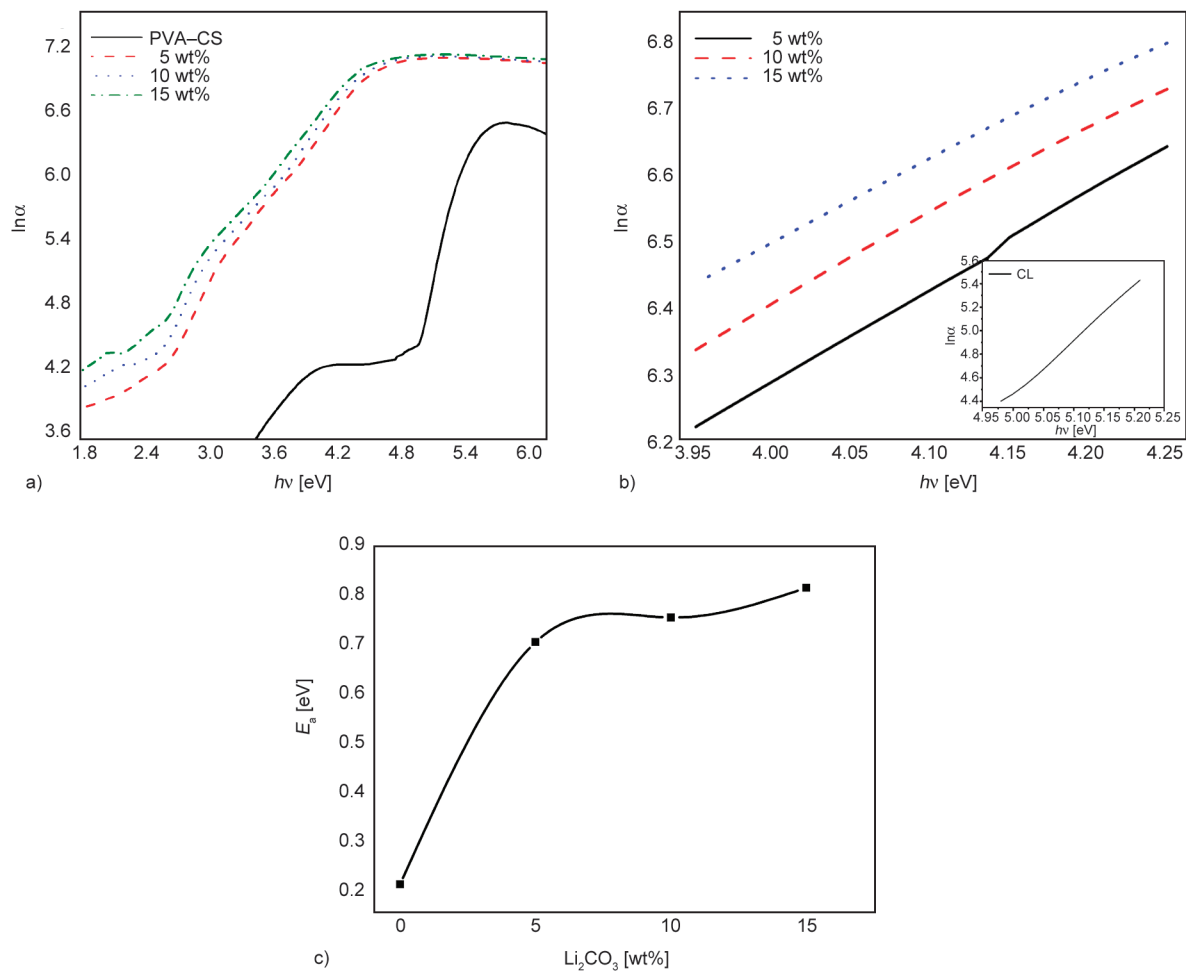


Figure 4. a) Variation of $\ln\alpha$ with $h\nu$ (photon energy), b) linear portion of $\ln\alpha$ vs. $h\nu$, and c) activation energy (E_a) vs. Li_2CO_3 doping concentrations.

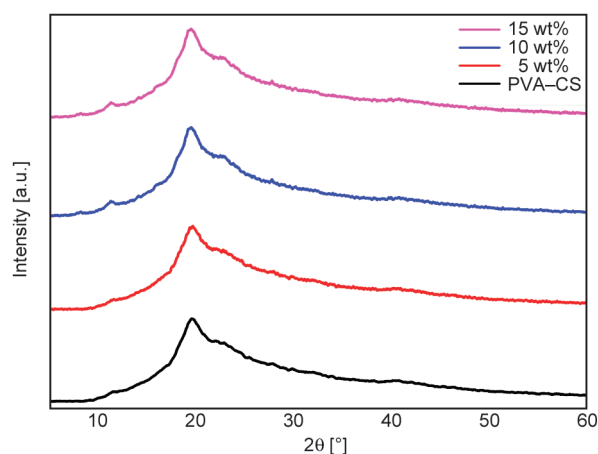
Table 2. UV–visible absorbance, optical energy band gap, and optical activation energy values of pure and salt-doped polymer blend composites.

Doping level, M [wt%]	λ_{max1} [nm]	λ_{max2} [nm]	λ_{edge1} [nm]	λ_{edge2} [nm]	E_g [eV]	E_a [eV]
0	206	303	248	354	4.69	0.21
5	242	–	472	–	2.99	0.70
10	247	–	528	–	2.91	0.75
15	251	–	540	–	2.85	0.81

E_a values for different dopant levels and their variations with salt concentrations are shown in Figure 4c and the same is tabulated in Table 2. From Figure 4c, it is observed that the E_a values increased with Li-salt doping concentration. Here, the ion mobility perception is responsible for the variation of Urbach's energy values in the case of doped polymer blend composites. This dopant provides additional defect states and forms complexes within the polymer blend matrix; by increasing doping concentration increases the density of localized states, which creates more and more additional defects and extends the mobility gap. Hence, the increased defects and complex formation enhance the Urbach's energy with an increase in salt concentration in the polymer matrix.

3.3. X-ray diffractometer studies (XRD)

The XRD instrument is a known tool to examine the crystal structure and yields appropriate information on the degree of crystallinity of the samples. The observed XRD pattern of pure and the salt-doped polymer blend composite are given in Figure 5, and the corresponding variations with salt concentration are in Table 3. From Figure 5, it is observed that, in the XRD pattern of pure PVA–CS polymer blend, a small

**Figure 5.** X-ray diffraction pattern of pure and Li-salt (5, 10, and 15 wt%) doped polymer blend composite.

peak is observed at 11.52° along with a broad peak spotted at 19.62° . Here the first peak centered at 11.52° is the corresponding characteristic peak of chitosan polymer, and another broad (highly intense) peak observed at 19.62° represents the semicrystalline nature of both PVA and chitosan polymers by comparing the diffraction peaks of pure and polymer blend composites in Figure 5. Figure 5 shows a modification and shifts in the characteristic peaks. For the Li-salt doped blend composites, it is observed that the intensity of the diffraction peak ($2\theta = 11.52^\circ$) increases with salt concentration.

Besides this, the intensity of the peak observed at 19.62° for pure polymer blend increases with salt concentration along with a slight shift towards the lower 2θ value. This modification in peak position and a slight shift in its position suggests that salt dissociation in the polymer matrix, as well as structural modification, takes place in the blend composites. These structural modifications that take place within the doped blend composite mainly arise due to the hydrogen bonding interaction between PVA–CS and Li-salt (FTIR studies). These interactions lead to the complex formation within the blend matrix whose number increases with doping concentration, which leads to the change of microstructural (crystalline/amorphous) nature in blend composites [14, 19]. To understand these structural modifications in the blend composites with doping level further, the degree of crystallinity (X_c) has been estimated for pure and doped blend composites using Hermans' and Weidinger formula (Equation (4)), [7, 8]:

$$X_c = \frac{A_c}{A_c + A_a} \cdot 100 \quad [\%] \quad (4)$$

where A_c represents areas of sharp crystalline peaks, A_a is the area of amorphous halos. The observed variations with doping concentrations are given in Table 3. From the table, it is observed that the crystallinity increases with an increase in Li_2CO_3 concentration in PVA–CS blend films; this is due to the formation of hydrogen bonding between Li_2CO_3 and polymer blend. The increased crystalline phase in composites clearly shows the interaction between the dopant and the polymer blend; these results are consistent with FTIR results.

The average crystallite size of PVA–CS and PVA–CS– Li_2CO_3 composites is calculated using Scherer's Equation (5):

Table 3. X-ray diffraction results of PVA–CS blend and PVA–CS–Li₂CO₃ electrolytes.

Sample PVA–CS + Li ₂ CO ₃ [wt%]	2θ [°]	d-spacing [Å]	P [nm]	R _s [Å]	Crystallinity, X _c [%]
0	11.52	8.929	0.589	9.920	48
	19.62	6.278	0.591	7.847	
	40.45	5.151	0.593	6.439	
5	11.56	10.59	0.973	7.385	56
	19.60	6.742	0.918	4.984	
	40.50	4.077	1.234	3.941	
10	11.56	3.235	0.842	5.709	58
	19.57	4.453	0.689	4.837	
	40.50	3.117	0.661	3.896	
15	11.57	3.869	0.865	5.482	61
	19.50	3.955	0.647	4.944	
	40.56	2.140	0.654	3.918	

$$P = \frac{K\lambda}{\beta} \cos \theta \quad (5)$$

where $K = 0.9$ is a constant, and it is related to the crystallite shape and miller indices of the reflecting crystallographic planes, λ – wavelength, β – FWHM (full width at half maximum) intensity of reflection in radians and θ – Bragg's angle [20, 21].

The average inter-crystallite separation for pure and Li-salt doped polymer blend composites is calculated using equations in references [22–24], Equation (6):

$$R_s = \frac{5\lambda}{8 \sin \theta} \quad (6)$$

The estimated crystallite size and inter-crystallite separation are tabulated in Table 3; the calculated crystallite size values show that it is increased with salt concentration. The table shows that the average crystallite separation in composites increases with salt concentration. Hence from the XRD pattern, it is clear that the microstructure of the pure polymer blend is modified due to the addition of Li₂CO₃.

3.4. Scanning electron microscopy (SEM)

Scanning electron microscopy (SEM) is employed to determine the nature of dopant dispersion in the polymer matrix. The observed SEM images of the pure polymer blend and different Li₂CO₃ concentrations (10 and 15 wt%) are presented in Figure 6. Figure 6a shows the smooth and homogenous surface attributed to the amorphous phase of the pure polymer blend, where the surface is clear, and there is no sign of any clusters on the surface of the polymer matrix. Figure 6b and Figure 6c shows the SEM images of Li-salt (10 and 15 wt%) doped polymer blend composites, here cluster formation on the

surface of the polymer matrix can be observed, and it increases with salt concentration which will be seen in Figure 6c [26].

This result indicates that the surface morphology of pure polymer blend is affected by the Li-salt doping and increases the surface roughness in doped polymer blend composites; this indicates the structural modification occurred due to salt doping (XRD results) [2, 22]. The increase in surface roughness with salt concentration is due to complexes formed through inter/intra-molecular interaction between functional groups of the polymer host and the dopant.

3.5. Thermogravimetric analysis (TGA)

The thermal property of pure and doped polymer composite films is studied using thermogravimetric analysis (TGA), where the mass loss percentage, phase transition, and decomposition temperature of pure and composite films are studied. Observed TGA graph of pure PVA–CS polymer blend and PVA–CS–Li₂CO₃ (5, 10, and 15 wt%) composite films are shown in Figure 7, and the mass loss values for pure and salt-doped polymer blend composite for different temperatures are tabulated in Table 4. The TGA curves (Figure 7) of pure and Li-salt doped polymer blend composites exhibit three stages of weight loss from 60–500 °C. The first stage of small weight loss for PVA–CS polymer blend is in the range of 60 to 140 °C (mass loss percentage ≈ 15%) and is assigned to the elimination of moisture within the film. Here the water molecules are bonded mainly to the amine or hydroxyl groups present in the polymer blend, which will easily be detached in this temperature range.

The second stage of mass loss (rapid decrease in mass loss ≈ of 45%) is the degradation stage, which

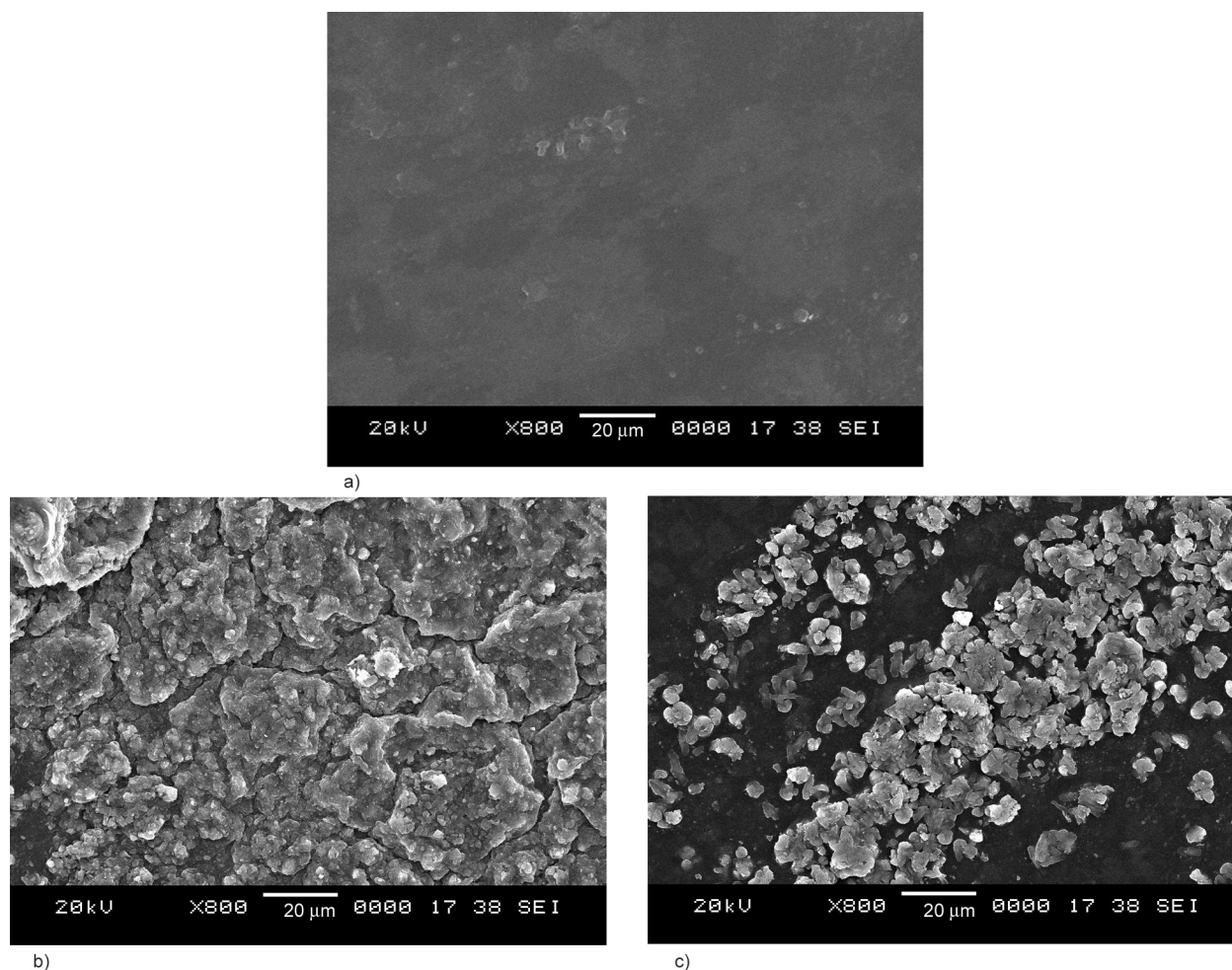


Figure 6. SEM images of a) PVA–CS polymer blend, b) PVA–CS–Li₂CO₃ (10 wt%), and c) PVA–CS–Li₂CO₃ (15 wt%).

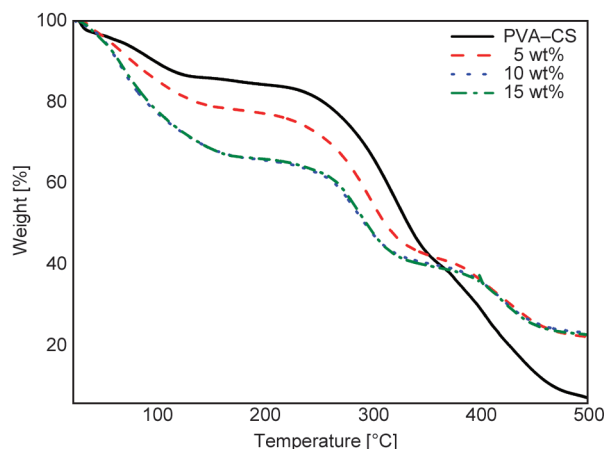


Figure 7. Thermogravimetric analysis of pure PVA–CS and PVA–CS–Li₂CO₃ (5, 10 and 15 wt%) blend composites.

begins at 220 °C and ends at 350 °C, where the structural modification takes place due to the decomposition of the polymer backbone chain. These structural modifications affect the crystalline phase of the pure polymer blend (XRD results), and the final degradation stage is between 360–480 °C (mass loss ≈35%)

Table 4. The weight loss percentage in pure and Li–salt doped polymer blend composites.

Li ₂ CO ₃ [wt%]	Weight loss [%]					T ₀ [°C]
	100 °C	200 °C	300 °C	400 °C	500 °C	
0	10.55	15.89	34.12	71.56	93.35	124
5	14.88	23.05	45.34	64.04	78.20	145
10	22.07	34.47	51.98	63.93	77.09	162
15	22.09	34.27	52.30	62.47	77.02	170

and is related to the decomposition of residues left within the pure blend [22, 23]. In blend composites, the first stage of mass loss (≈12%) is observed between 70–150 °C, which is due to the evaporation of moisture present in the composite films. The second stage (degradation) occurs between 260–390 °C (mass ≈25% for 15 wt%, Li₂CO₃), which is due to the chain scission of the polymer backbone and splitting of bonds between dopant and polymer backbone, and the final degradation stage occurs between 400–500 °C (mass loss ≈20%). Also, from the table, it is observed that the mass loss values of composite films decrease compared with the pure polymer blend film.

That is compared to the mass loss of pure blend, and in Li–salt (15 wt%) doped polymer blend composite, first stage mass loss decreases from 15 to 12%, for the second stage of mass loss varies from 40 to 25% and the final degradation stage decreased from 35% to 20%. These results show that the thermal stability of the polymer blend films increases with doping. This indicates the increase of thermal stability of the doped blend composite films due to the chemical degradation process via chain scission in the polymer backbone. Hence from the TGA graph, it is observed that the thermal stability of the PVA–CS polymer blend is increased after adding Li_2CO_3 salt [24].

3.6. Impedance analysis studies

The impedance analysis is one of the familiar techniques used to study the charging and transport phenomenon in conducting and conjugated polymer composites. Figure 8a shows the observed Cole–Cole plot of the PVA–CS polymer blend and Li_2CO_3 doped polymer blend electrolytes. The Cole–Cole plot of pure polymer blend and doped samples comprises a broad semi-circle or oblique region at the high-frequency window and a tail (linear region) at the low-frequency region. Here, the semi-circle corresponds to the bulk conductivity of the polymer electrolytes, and the linear region attributes to double-layer capacitance at the electrode/electrolyte interface. The semi-circle arises due to the parallel combination of bulk capacitance and bulk resistance of the electrolyte films [25, 26]. From the plot, it is observed that the semi-circle decreases with an increase in Li–salt concentration and the low-frequency linear region appeared as a spike which inclined at an angle less than 90° along the real axis. The variation in the plot indicates the decrease of resistance for charge

carriers in the electrolyte films, which is due to the ion migration through the free volume of the polymer electrolytes.

To understand the ionic conduction in the polymer electrolytes, the relaxation time (τ) of polymer blend electrolyte films is calculated using the relation (Equation (7)):

$$\tau = \frac{1}{\omega} \tag{7}$$

where $\omega = 2\pi f_{\text{max}}$, here f_{max} is relaxation frequency (maximum frequency of the imaginary part of impedance peak) displayed in Figure 8b. Here, no relaxation peaks are observed for the pure polymer blend. This is because the experiment was conducted in the frequency range 40 Hz–5 MHz, and the relaxation peaks of these samples lay below 40 Hz, which is due to the hindrance in mobile charge carriers within the matrix. For salt–doped polymer blend electrolytes, the relaxation peaks appear and shift towards a higher frequency region with an increase of dopant concentration up to 15 wt%. From Figure 9, one can clearly observe

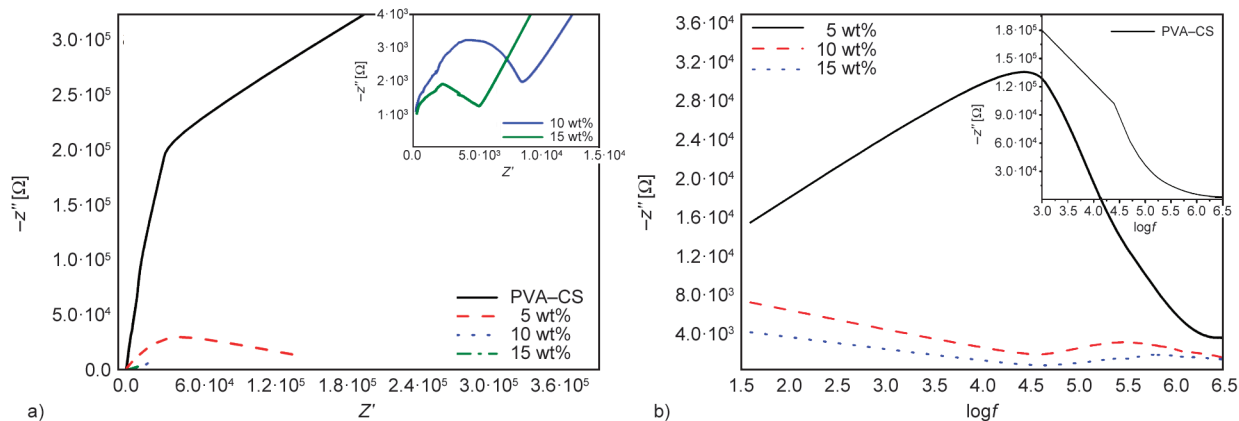


Figure 8. a) Cole–Cole plot, and b) imaginary part of impedance vs. $\log f$, of pure and Li–salt doped blend polymer electrolyte system.

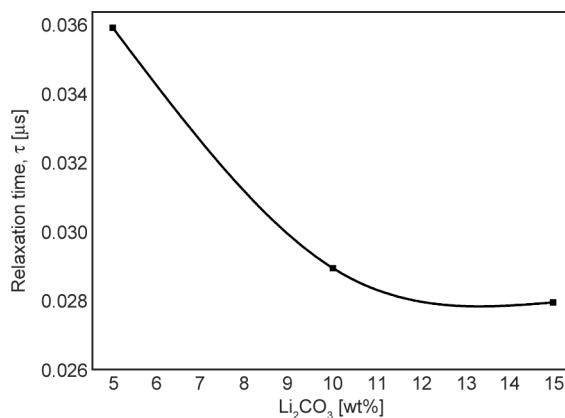


Figure 9. Variation of relaxation time of Li–salt doped PVA–CS polymer blend electrolyte.

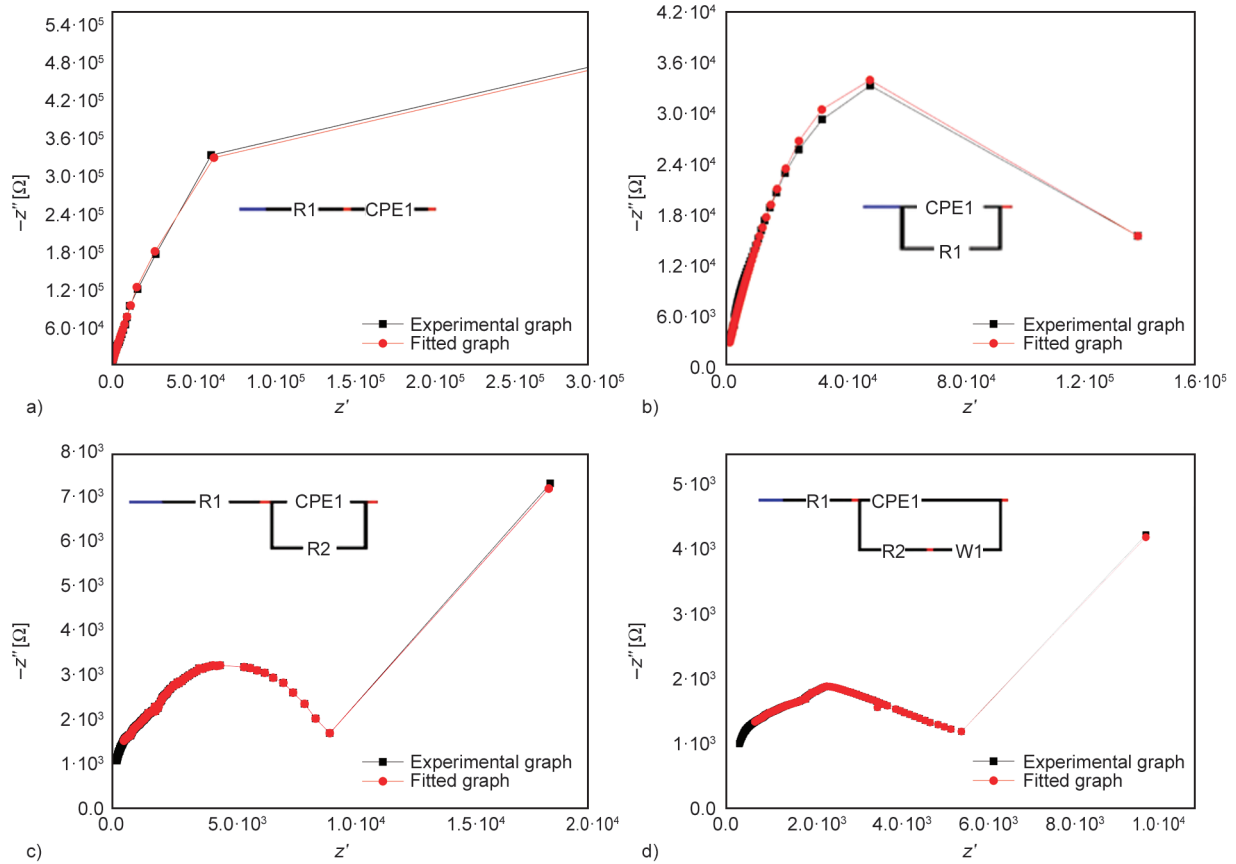


Figure 10. Fitted graph of a) PVA–CS, b) Li_2CO_3 (5 wt%), c) Li_2CO_3 (10 wt%), and d) Li_2CO_3 (15 wt%).

that the τ value is decreased upon doping; as a result, surging of mobile charge carriers takes place within the electrolyte films. Hence such mobile charge carriers are responsible for the conduction mechanism within the doped polymer blend electrolytes [27].

Figure 10 shows the Cole–Cole plot of experimental data and equivalent circuit-fitted data using electrochemical impedance spectroscopy (EIS spectrum analyzer) for pure PVA–CS, and different concentrations of Li–salt (5, 10, and 15 wt%) doped polymer blend electrolytes. From Figure 10 it is observed that

the fitted impedance data is in good agreement with the experimental impedance data.

The Cole–Cole plot for a high–conducting polymer blend electrolyte (Li_2CO_3 , 15 wt%) is studied for different temperatures (Figure 11a). From Figure 11 it is observed that there is a significant decrease in the size of the semi–circle with an increase in temperature. This shows the decrease in the resistive nature of the polymer blend electrolyte system. At higher temperatures, the semi–circle relatively disappeared; as a result, the ionic resistance of the polymer blend

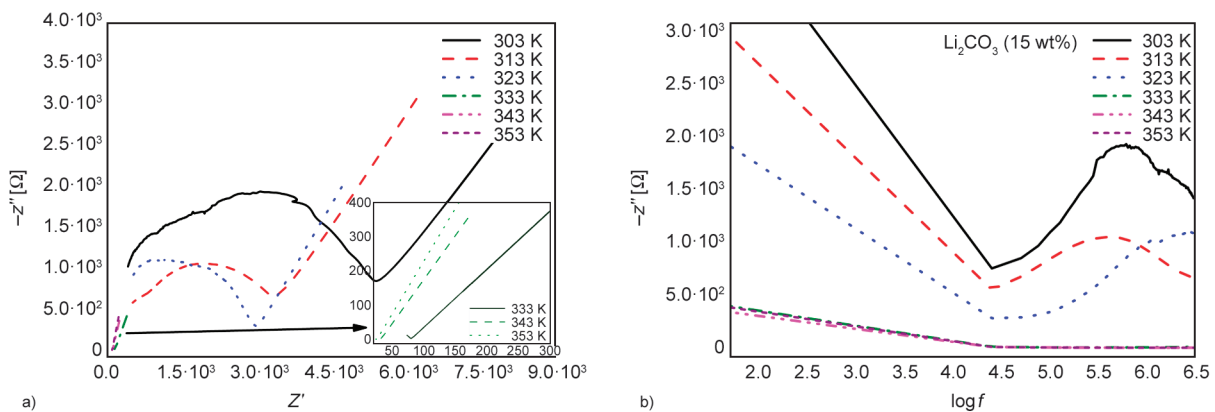


Figure 11. a) Cole–Cole plot, and b) imaginary part of impedance (Z'') versus $\log f$, of Li–salt (15 wt%) doped PVA–CS blend electrolyte for different temperatures.

electrolyte system falls to a very small value at high temperatures. The decrease in resistance at high temperatures is related to the concept that, as temperature increases, the polymer backbone chain becomes more flexible, which promotes the segmental motion of polymer chain segments within the blend electrolyte system and increases the disassociation of salt within the polymer matrix [27, 28]. So that the ionic mobility increases with temperature, hence the enhancement of ionic conductivity in doped polymer blends.

The logical reason for the increase of conductivity in doped polymer blend electrolytes compared to a single polymer-based SPBE system is that the polymer blend electrolytes have more capacity for salt disassociation within the blend matrix. Since more disassociation of salt within the polymer blend matrix facilitates maximum ionic movement, hence conductivity enhances [22]. Figure 11b shows the relaxation peak of mobile charge carriers for different temperatures. The relaxation peaks are observed for

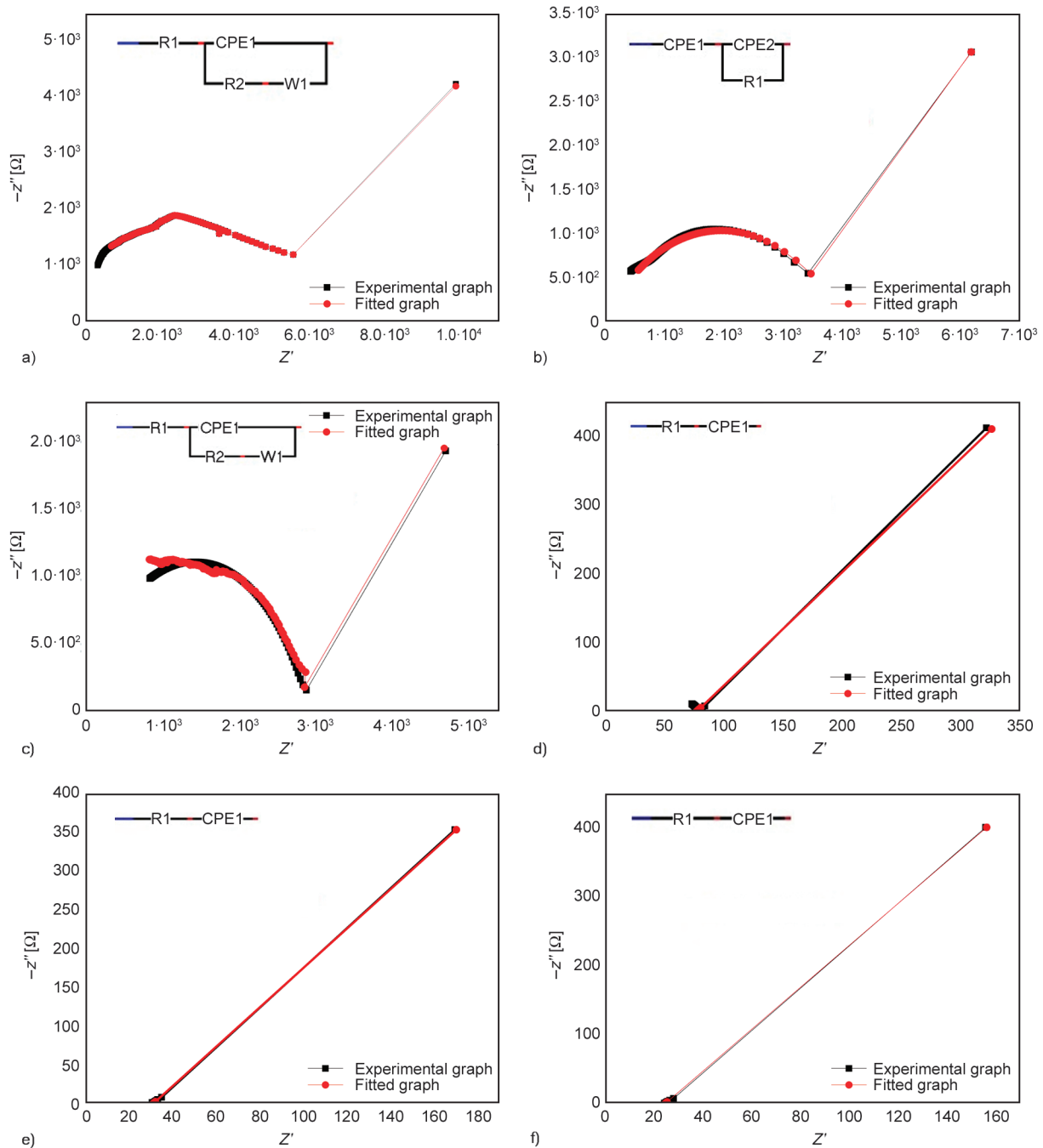


Figure 12. Fitted graph of Li_2CO_3 (15 wt%) for different temperatures, a) 303 K, b) 313 K, c) 323 K, d) 333 K, e) 343 K, and f) 353 K.

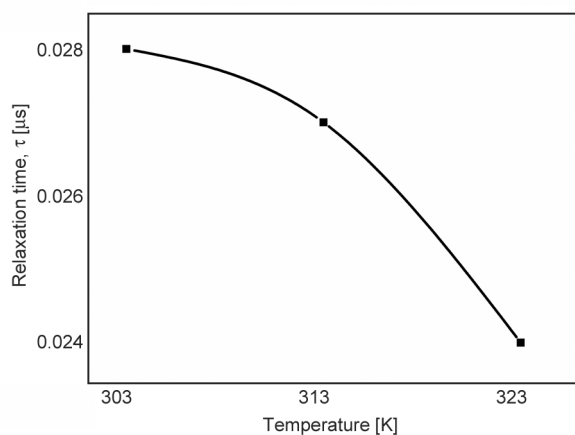


Figure 13. Variation of relaxation time of Li-salt (15 wt%) doped PVA-CS polymer blend electrolyte for different temperatures.

high-conducting polymer blend electrolytes exhibiting enhancement in conductivity at different temperatures. Whereas at low temperatures, the relaxation peaks are appeared because of immobile charge carriers and for high temperatures, the relaxation peaks are observed due to the formation of defects caused by the temperature. Figure 12 exhibits the Cole-Cole plot of experimental and the equivalent circuit-fitted data using electrochemical impedance spectroscopy (EIS spectrum analyzer) of the high conducting (Li_2CO_3 , 15 wt%) polymer blend electrolyte film for different temperatures. From the Figure 12 it is clearly observed that the fitted impedance data is in good agreement with the experimental impedance data of the prepared polymer electrolyte film. Figure 13 shows the variation of the relaxation time of ions with respect to temperature; here, it is observed that the τ value decreased with an increase in temperature.

3.7. Electrical properties

The ionic conductivity in SPEs depends on the mobility and concentration of the charge carriers. By using the measured dielectric parameters, the ac-conductivity of the polymer blend and Li_2CO_3 doped polymer electrolyte films are calculated using the Equation (8):

$$\sigma_{ac} = 2\pi f \epsilon_0 \epsilon_r \tan \delta \quad (8)$$

where f is the applied frequency, ϵ_0 the permittivity in free space, ϵ_r the dielectric constant, and $\tan \delta$ is the dielectric loss [18]. The frequency-dependent ionic conductivity of pure and Li_2CO_3 doped polymer blend electrolytes are depicted in Figure 14.

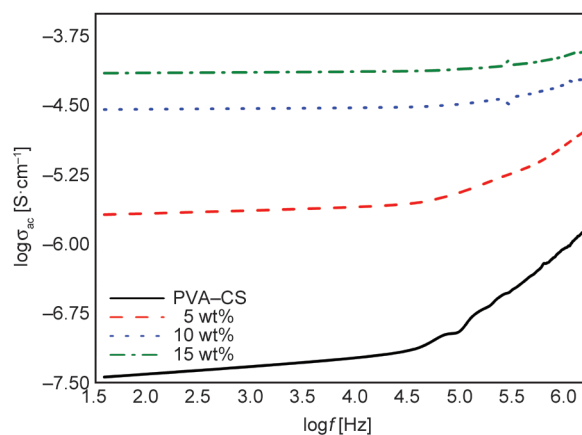


Figure 14. Variation of $\log \sigma_{ac}$ with the frequency of PVA-CS and Li-salt doped polymer blend.

From Figure 14 it is observed that the conductivity of pure polymer blend is relatively low, and it enhances with an increase of frequency. The increase of conductivity is attributed to the fact that when an alternating field is applied across the electrodes, the flexibility of bonds increases, in turn, makes the polymer chains flexible. As a result, a significant increase in the mobility of ions within the electrolytes is expected, which leads to an increase in ionic conductivity and is apparently observed at higher frequency regions. From Figure 14 it is observed that two distinct regions are observed over the measured frequency range. One is the low-frequency plateau region that tends to approach dc-conductivity at zero frequency, and the other is the high-frequency dispersion region which is attributed to ac-conductivity [29]. The conductivity is relatively poor at the plateau region which is due to the electrode polarization; here, the mobility of ions is hindered because of the accumulation of mobile charge carriers at the electrode/electrolyte interface. Whereas as the frequency increases, the bonds present in the polymer blend matrix rotate along with the frequency, which facilitates the segmental motion of polymer chains. As a result of this, the ions are adequately energized to move from one conducting site to another, which leads to the enhancement of conductivity at higher frequency regions. The ionic conductivity also enhances with an increase of dopant concentration which is attributed to the fact that the interaction between functional groups of dopant and the polymer blend creates the void between the nearest localized states, resulting in the lowering of the potential barrier within them. As a result, more and more ionic transfer took place between these localized states [30],

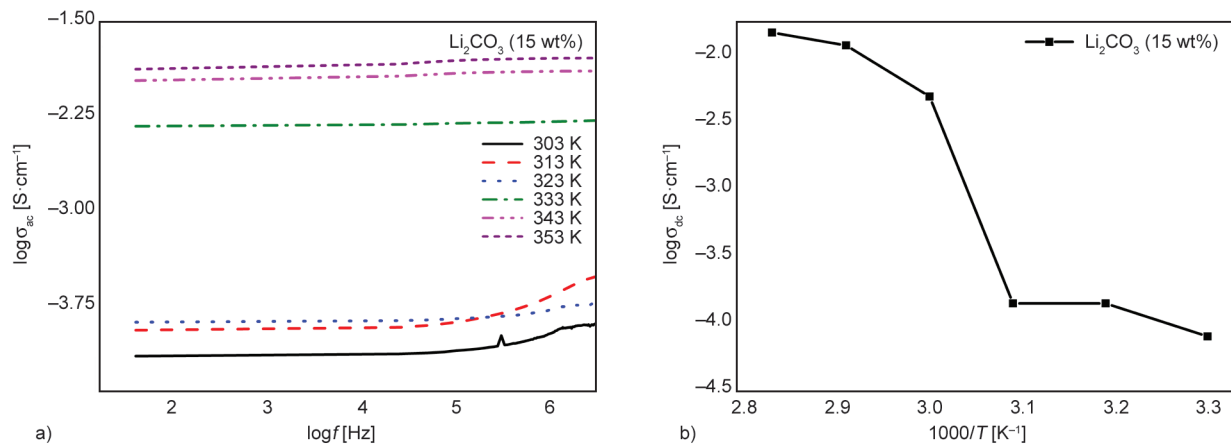


Figure 15. a) $\log \sigma_{ac}$ -conductivity vs. $\log f$, b) $\log \sigma_{dc}$ vs. $1000/T$ of high conducting polymer blend electrolyte film (Li₂CO₃, 15 wt%) for different temperatures.

and hence the enhancement of ionic conductivity is observed in polymer blend electrolytes. The maximum ionic conductivity obtained is $7.70 \cdot 10^{-5} \text{ S} \cdot \text{cm}^{-1}$ (15 wt%, Li₂CO₃).

The highest conducting polymer blend electrolyte is studied with different temperatures as a function of frequency, which is depicted in Figure 15a. The variation of ionic conductivity with frequency follows Jonscher’s universal power law (Equation (9)):

$$\sigma_{ac} = \sigma_{dc} + A\omega^s \quad (9)$$

where σ_{dc} is the DC conductivity is obtained by extrapolating the low-frequency region to the y-axis ($\log \sigma_{ac}$), A is the pre-exponential factor, and s the frequency exponent factor ranging from 0 to 1. From Figure 15 it is observed that the conductivity increases with an increase in temperature as well as frequency. The increase in ionic conductivity with temperature is interpreted in terms of the hopping mechanism, polymer chain segmental motion, and local structural relaxation [22, 31]. As temperature increases, the complex sites within the electrolyte system increase, enabling ions to jump from one conducting site to another. Hence the conductivity increases with temperature, and the highest dc-conductivity is observed at 353 K, *i.e.* $\sigma = 1.42 \cdot 10^{-2} \text{ S} \cdot \text{cm}^{-1}$. Figure 15b shows the Arrhenius plot (dc-conductivity vs. temperature inverse) of Li₂CO₃ (15 wt%) doped PVA–CS polymer blend electrolyte system. After 303 K, the observed sudden increase in conductivity is attributed to the transition of the polymer crystalline/semicrystalline phase to the amorphous phase upon doping [32]. As a result, ionic motion (an interchain hopping mechanism) takes place in the doped electrolyte

system; thus, the highest dc-conductivity is observed at 353 K.

3.8. Transport properties

The transference numbers corresponding to the ionic (t_{ion}) and electronic (t_{ele}) transport for Li₂CO₃ (15 wt%) doped polymer blend electrolyte film has been investigated using Wagner’s polarization technique. According to the method, the highest conducting polymer blend electrolyte was sandwiched between two silver electrodes under the fixed dc-voltage of 1 V and the corresponding dc polarization current was measured as a function of time for the 15% Li₂CO₃ doped PVA–CS polymer. Figure 16 shows the observed variation of polarization current with time. From this figure, it can be seen that the initial large current I_i is the contribution of both ions as well as electrons. Then as time proceeds, the current decreases and reaches a steady state after a few

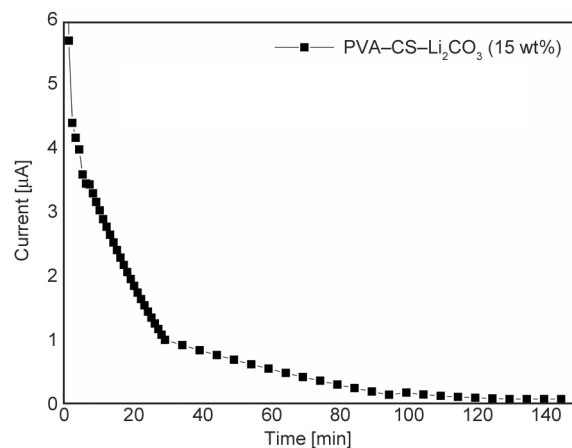


Figure 16. Variation of polarization current with time for Li₂CO₃ doped PVA–CS polymer blends composite film.

minutes of polarization, and at the steady state, the current conduction is due to electrons alone I_f .

The ion transport number is said to be the ratio of any particle/ion transference number to total conductivity, and for electronic transference, the number is the ratio of electron/hole transference number to total conductivity. The corresponding ionic (t_+) and electronic (t_-) transference numbers are calculated using Equations (10) and (11):

$$t_+ = \frac{I_i - I_f}{I_i} \quad (10)$$

$$t_- = \frac{I_f}{I_i} \quad (11)$$

where I_i is the initial current and I_f is the final current. The observed total ion transference number in Li_2CO_3 (15 wt%) doped polymer blend composite film is 0.95, and the ions transfer number is 0.05; this shows the ions play a major role in the conduction mechanism within the blend electrolyte, compared to electron's contribution for conduction. From the observed results, it is concluded that the ions are the majority charge carriers in Li_2CO_3 doped polymer blend composite. Hence this kind of blend electrolyte film is suitable for the fabrication of energy storage device applications [32, 33].

3.9. Diffusion coefficient

To understand the ionic mobility, the total ionic mobility in the SPE system can be divided into cationic and anionic mobility. It is difficult to determine the exact mobility of charge carriers in the polymer electrolyte system because most of them are bounded to ion pairs. These can be estimated by using the following equations, the diffusion coefficient and mobility of ions in polymer electrolyte are calculated using (Equations (12) and (13)):

$$D = \frac{kT\sigma}{ne^2} \quad (12)$$

$$\mu = \frac{\sigma}{ne} \quad (13)$$

where k is the Boltzmann constant, T the temperature, σ the ionic conductivity, n is the number molecules present [cm^{-3}], and e is the charge of an electron. The diffusion coefficients (D_+ and D_-), cationic (μ_+), and anionic (μ_-) mobility for PVA–CS+ Li_2CO_3 polymer electrolyte system is determined using equations described in the literature [34] and are listed in Table 5. From Table 5, it is observed that the cationic mobility and diffusion coefficients are high compared to that of anions. From these results, it affirms that the ionic conductivity is strongly influenced by cationic motion and the diffusion coefficient of cations within the electrolyte system [32, 35]. Hence the ionic conduction in Li_2CO_3 doped polymer blend electrolyte is mainly due to cations. The increase in mobile charge carriers within the electrolyte films causes increases in the ionic conductivity of the electrolyte films.

4. Conclusions

In this study, the pure and Li–salt doped polymer blend composites are prepared by the solution cast method. From FTIR studies, the inter/intra-molecular interaction between Li_2CO_3 and PVA–CS takes place due to the collegial effect of hydrogen bonds in polymer blend and Li_2CO_3 , and forms charge transfer complexes within the electrolyte films. XRD studies confirm the structural modifications that take place after doping Li_2CO_3 , and it is clearly shown that the crystallinity in composites is gradually increased compared to a pristine polymer blend. The SEM images shows the formation of clusters at higher Li_2CO_3 (10 and 15 wt%) concentrations, which increases the surface roughness of the blend. In TGA studies, the increase in mass loss percentage with temperature confirms the increased thermal stability of the PVA–CS polymer blend due to doping. From the impedance analysis, it is confirmed that the mobility of charge carriers increases, and the relaxation time of mobile charge carriers decreases with Li_2CO_3 concentration. The ac–conductivity study revealed that the conductivity of the blend increases with the doping level; the highest conductivity is achieved for 15 wt% of Li_2CO_3 concentration. The

Table 5. Transference number, ionic mobility, and diffusion coefficient of 15 wt% Li_2CO_3 doped PVA–CS polymer electrolyte.

Weight ratio	t_+	t_-	μ_+ [$\text{cm}^2 \cdot \text{V}^{-1} \cdot \text{s}^{-1}$]	μ_- [$\text{cm}^2 \cdot \text{V}^{-1} \cdot \text{s}^{-1}$]	D_+ [$\text{cm}^2 \cdot \text{s}^{-1}$]	D_- [$\text{cm}^2 \cdot \text{s}^{-1}$]
Li_2CO_3 (15 wt%)	0.96	0.04	$7.164 \cdot 10^{-7}$	$0.253 \cdot 10^{-7}$	$1.426 \cdot 10^{-9}$	$0.023 \cdot 10^{-9}$

transport properties reveal that the ionic transference number is more than the electronic transference number within the blended composite.

Acknowledgements

The authors are thankful to PURSE laboratory, Microtron center, and University Science Instrumentation Center (USIC), Mangalore University for providing UV–Visible spectroscopy, Fourier transforms infrared spectroscopy (FTIR), Thermo gravimetric analysis (TGA), and scanning electron microscopy (SEM), and impedance analyzer. The authors are also thankful to the innovation center MIT, Manipal for providing an X-ray diffractometer (XRD).

References

- [1] Zheng H., Du Y., Yu J., Huang R., Zhang L.: Preparation and characterization of chitosan/poly(vinyl alcohol) blend fibers. *Journal of Applied Polymer Science*, **80**, 2558–2565 (2001).
<https://doi.org/10.1002/app.1365>
- [2] Salman Y. A. K., Abdullah O. Gh., Hanna R. R., Aziz S. B.: Conductivity and electrical properties of chitosan – methylcellulose blend biopolymer electrolyte incorporated with lithium tetrafluoroborate. *International Journal of Electrochemical Science*, **13**, 3185–3199 (2018).
<https://doi.org/10.20964/2018.04.25>
- [3] Shukur M. F., Ithnin R., Illias H. A., Kadir M. F. Z.: Proton conducting polymer electrolyte based on plasticized chitosan–PEO blend and application in electrochemical devices. *Optical Materials*, **35**, 1834–1841 (2013).
<https://doi.org/10.1016/j.optmat.2013.03.004>
- [4] de Souza Costa–Junior E., Pereira M. M., Mansur H. S.: Properties and biocompatibility of chitosan films modified by blending with PVA and chemically cross-linked. *Journal of Materials Science: Materials in Medicine*, **20**, 553–561 (2009).
<https://doi.org/10.1007/s10856-008-3627-7>
- [5] Yusof Y. M., Illias H. A., Kadir M. F. Z.: Incorporation of NH₄Br in PVA–chitosan blend–based polymer electrolyte and its effect on the conductivity and other electrical properties. *Ionics*, **20**, 1235–1245 (2014).
<https://doi.org/10.1007/s11581-014-1096-1>
- [6] Islam A., Imran Z., Yasin T., Gull N., Khan S. M., Shafiq M., Sabir A., Munawar M. A., Raza M. H., Jamil T.: An investigation of AC impedance and dielectric spectroscopic properties of conducting chitosan–silane cross-linked–poly (vinyl alcohol) blended films. *Materials Research*, **18**, 1256–1263 (2015).
<https://doi.org/10.1590/1516-1439.043715>
- [7] Bhajantri R. F., Ravindrachary V., Poojary B., Ismayil., Harisha A., Crasta V.: Studies on fluorescent PVA + PVP + MPDMAPP composite films. *Polymer Engineering and Science*, **49**, 903–909 (2009).
<https://doi.org/10.1002/pen.21341>
- [8] Sagar R. N., Ravindrachary V., Guruswamy B., Hegde S., Mahanthesh B. K., Ku-mari R. P.: Effect of TiO₂ nanoparticles doping on structural and electrical properties of PVA: NaBr polymer electrolyte. *AIP Conference Proceedings*, **1953**, 030216 (2018).
<https://doi.org/10.1063/1.5032551>
- [9] Xu G., Xu G., Shi T.: Grafting of chitosan Schiff base on graphene oxide and its characterization. *Fullerenes, Nanotubes and Carbon Nanostructures*, **24**, 749–756 (2016).
<https://doi.org/10.1080/1536383X.2016.1226285>
- [10] Buraidah M. H., Teo L. P., Majid S. R., Arof A. K.: Ionic conductivity by correlated barrier hopping in NH₄I doped chitosan solid electrolyte. *Physica B*, **404**, 1373–1379 (2009).
<https://doi.org/10.1016/j.physb.2008.12.027>
- [11] Khiar A. S. A., Puteh R., Arof A. K.: Characterizations of chitosan-ammonium triflate (NH₄CF₃SO₃) complexes by FTIR and impedance spectroscopy. *Physica Status Solidi*, **203**, 534–543 (2006).
<https://doi.org/10.1002/pssa.200521016>
- [12] Ismayil., Ravindrachry V., Bhajantri R. F., Praveena S. D., Poojari B., Dutta D., Pujari P. K.: Optical and microstructural studies on electron irradiated PMMA: A positron annihilation study. *Polymer Degradation and Stability*, **95**, 1083–1091 (2010).
<https://doi.org/10.1016/j.polymdegradstab.2010.02.031>
- [13] Thripathi S., Mehrotra G. K., Dutta P. K.: Preparation and physicochemical evaluation of chitosan/poly(vinyl alcohol)/pectin ternary film for food-packaging applications. *Carbohydrate Polymers*, **79**, 711–716 (2010).
<https://doi.org/10.1016/j.carbpol.2009.09.029>
- [14] Aziz S. B., Abdullah R. M., Rasheed M. A., Ahmed H. M.: Role of ion dissociation on DC conductivity and silver nanoparticle formation in PVA:AgNt based polymer electrolytes: Deep insights to ion transport mechanism. *Polymers*, **9**, 338 (2017).
<https://doi.org/10.3390/polym9080338>
- [15] Al-Gunaid M. Q. A., Saeed A. M. N., Subramani N. K., Madhukar B. S., Siddaramaiah: Optical parameters, electrical permittivity and *I–V* characteristics of PVA/Cs₂CuO₂ nanocomposite films for opto-electronic applications. *Journal of Materials Science: Materials in Electronics*, **28**, 8074–8086 (2017).
<https://doi.org/10.1007/s10854-017-6513-6>
- [16] Han D., Yan L., Chen W., Li W.: Preparation of chitosan/graphene oxide composite film with enhanced mechanical strength in the wet state. *Carbohydrate Polymers*, **83**, 653–658 (2011).
<https://doi.org/10.1016/j.carbpol.2010.08.038>
- [17] Ali H., Tiama T. M., Ismail A. M.: New and efficient NiO/chitosan/polyvinyl alcohol nanocomposites as antibacterial and dye adsorptive films. *International Journal of Biological Macromolecules*, **186**, 278–288 (2021).
<https://doi.org/10.1016/j.ijbiomac.2021.07.055>

- [18] Hegde S., Ravindrachary V., Praveena S. D., Guruswamy B., Sagar R. N.: Optical and dielectric properties of Li⁺ ion conducting solid polymer electrolyte. *Indian Journal of Advances in Chemical Science*, **6**, 83–87 (2018).
<https://doi.org/10.22607/IJACS.2018.602004>
- [19] Aziz S. B., Hamsan M. H., Nofal M. M., Karim W. O., Brevik I., Brza M. A., Abdulwahid R. T., Al-Zangana S., Kadir M. F. Z.: Structural, impedance and electrochemical characteristics of electrical double layer capacitor devices based on chitosan: Dextran biopolymer blend electrolytes. *Polymers*, **12**, 1411 (2020).
<https://doi.org/10.3390/polym12061411>
- [20] Praveena S. D., Ravindrachary V., Bhajantri R. F., Ismayil: Dopant-induced microstructural, optical, and electrical properties of TiO₂/PVA composite. *Polymer Composites*, **37**, 987–997 (2016).
<https://doi.org/10.1002/pc.23258>
- [21] Yahia I. S., Mohammed M. I., Nawar A. M.: Multifunction applications of TiO₂/poly(vinyl alcohol) nanocomposites for laser attenuation applications. *Physica B: Condensed Matter*, **556**, 48–60 (2019).
<https://doi.org/10.1016/j.physb.2018.12.031>
- [22] Hegde S., Ravindrachary V., Praveena S. D., Ismayil, Guruswamy B., Sagar R. N.: Microstructural, dielectric, and transport properties of proton-conducting solid polymer electrolyte for battery applications. *Ionics*, **26**, 2379–2394 (2020).
<https://doi.org/10.1007/s11581-019-03383-w>
- [23] Yang J.-M., Wang S.-A.: Preparation of graphene-based poly(vinyl alcohol)/chitosan nanocomposites membrane for alkaline solid electrolytes membrane. *Journal of Membrane Science*, **477**, 49–57 (2015).
<https://doi.org/10.1016/j.memsci.2014.12.028>
- [24] Abdelaziz M.: Cerium (III) doping effects on optical and thermal properties of PVA films. *Physica B: Condensed Matter*, **406**, 1300–1307 (2011).
<https://doi.org/10.1016/j.physb.2011.01.021>
- [25] Kathayat K., Panigrahi A., Pandey A., Kar S.: Characterization of electrical behavior of Ba₅HoTi₃V₇O₃₀ ceramic using impedance analysis. *Materials Sciences and Applications*, **3**, 390–397 (2012).
<https://doi.org/10.4236/msa.2012.36056>
- [26] Al-Gunaid M. Q. A., Saeed A. M. N., Siddaramaiah: Effects of the electrolyte content on the electrical permittivity, thermal stability, and optical dispersion of poly(vinyl alcohol)–cesium copper oxide–lithium perchlorate nanocomposite solid-polymer electrolytes. *Journal of Applied Polymer Science*, **135**, 45852 (2017).
<https://doi.org/10.1002/app.45852>
- [27] Shukur M. F., Ithin R., Kadir M. F. Z.: Electrical properties of proton conducting solid biopolymer electrolytes based on starch–chitosan blend. *Ionics*, **20**, 977–999 (2014).
<https://doi.org/10.1007/s11581-013-1033-8>
- [28] Prajapati G. K., Roshan R., Gupta P. N.: Effect of plasticizer on ionic transport and dielectric properties of PVA–H₃PO₄ proton conducting polymeric electrolytes. *Journal of Physics and Chemistry of Solids*, **71**, 1717–1723 (2010).
<https://doi.org/10.1016/j.jpics.2010.08.023>
- [29] Dhayal V., Hashmi S. Z., Kumar U., Choudhary B. L., Kuznetsov A. E., Dalela S., Kumar S., Kaya S., Dolia S. N., Alvi P. A.: Spectroscopic studies, molecular structure optimization and investigation of structural and electrical properties of novel and biodegradable chitosan–GO polymer nanocomposites. *Journal of Material Science*, **55**, 14829–14847 (2020).
<https://doi.org/10.1007/s10853-020-05093-5>
- [30] Mahendia S., Goyal P. K., Tomar A. K., Chahal R. P., Kumar S.: Study of dielectric behavior and charge conduction mechanism of poly(vinyl alcohol) (PVA)-copper (Cu) and gold (Au) nanocomposites as a bio-resorbable material for organic electronics. *Journal of Electronic Materials*, **45**, 5418–5426 (2016).
<https://doi.org/10.1007/s11664-016-4677-0>
- [31] Aziz S. B., Abdullah O. Gh., Hussein S. A., Ahmed H. M.: Effect of PVA blending on structural and ion transport properties of CS:AgNt-based polymer electrolyte membrane. *Polymers*, **9**, 622 (2017).
<https://doi.org/10.3390/polym9110622>
- [32] Sagar R. N., Ravindrachary V., Hegde S., Guruswamy B.: Transport and diffusion properties in PEO–BaCl₂ polymer electrolytes for battery applications. *IOP Conference Series: Journal of Physics*, **1172**, 012078 (2019).
<https://doi.org/10.1088/1742-6596/1172/1/012078>
- [33] Shukur M. F., Kadir M. F. Z.: Hydrogen ion conducting starch–chitosan blend based electrolyte for application in electrochemical devices. *Electrochimica Acta*, **158**, 152–165 (2015).
<https://doi.org/10.1016/j.electacta.2015.01.167>
- [34] Francis K. M. G., Subramanian S., Shunmugavel K., Naranappa V., Pandian S. S. M., Nadar S. C.: Lithium ion–conducting blend polymer electrolyte based on PVA–PAN doped with lithium nitrate. *Polymer–Plastics Technology and Engineering*, **55**, 25–35 (2016).
<https://doi.org/10.1080/03602559.2015.1050523>
- [35] Leena Chandra M. V., Karthikeyan S., Selvasekarapandian S., Vinoth Pandi D., Monisha S., Arulmozhi Packiaseeli S.: Characterization of high ionic conducting PVAc–PMMA blend–based polymer electrolyte for electrochemical applications. *Ionics*, **22**, 2409–2420 (2016).
<https://doi.org/10.1007/s11581-016-1763-5>